ATLAS NOTE

ATLAS-CONF-2016-002

29th February 2016

Studies of b-tagging performance and jet substructure in a high p_{T} $g \to b\bar{b}$ rich sample of large-R jets from pp collisions at $\sqrt{s} = 8$ TeV with the ATLAS detector

The ATLAS Collaboration

ATLAS-CONF-2016-002
29 February 2016

Abstract

This note summarizes studies of b-tagging performance and the modeling of jet properties in high p_{T}, double b-tagged, large-R jets from $\sqrt{s} = 8$ TeV pp collisions collected using the ATLAS detector at the Large Hadron Collider. The double b-tag requirement yields a sample rich in jets originating from the $g \to b\bar{b}$ process. Using this sample, the performance of b-tagging at small b-quark angular separations is probed, and the modeling of jet properties, including substructure variables, is examined. Good agreement between data and Monte Carlo simulation is found within the experimental uncertainties.

1 Introduction

The identification of jets containing b-hadrons is of paramount importance to a host of measurements and new physics searches with the ATLAS experiment [1] at the LHC. Amongst the most important for Run 2 of the LHC are the identification and measurement of the Standard Model Higgs boson decay to $b\bar{b}$ pairs. The purest sample of Standard Model $H \to b\bar{b}$ events is found when the Higgs boson is produced with significant transverse momentum, or boost [2]. Despite the low acceptance of this kinematic regime, the background reduction is greater than at lower boson momenta and the significance is correspondingly higher. The boosted topology is additionally important in searches for new heavy resonances decaying to Higgs bosons, where the Higgs bosons are produced with high transverse momentum for resonances with masses greater than 800 GeV [3]. This boost causes the b-quarks to have a small angle between them and the fragmentation and hadronization products merge into one jet. While standard identification techniques of jets containing b-hadrons, termed b-tagging, have been studied in detail and calibrated in data [4, 5], such work has mainly focused on b-tagging in environments where the jets are relatively isolated from other hadronic activity. These techniques been studied in boosted top-antitop quark environments [6] but not in dense double b-quark jets environments. In addition, large radius jet and jet substructure techniques are frequently used to capture the Higgs boson decay products into a single jet in order to measure the Higgs boson candidate kinematics [7]. The mass and energy of these jets have been calibrated, and the corresponding uncertainties have been estimated, in inclusive multi-jet event samples which rarely contain two b-quark jets [7]. Therefore, it is vital to understand if the b-tagging performance studies and calibrations, as well as the large-R jet calibrations and uncertainties, are valid for topologies containing two close-by b-hadrons.

In order to validate the jet and b-tagging performance in the boosted regime, this analysis uses a set of events enriched with large-R jets containing two b-hadrons. This topology is selected from events collected by standard jet triggers by requiring a large-R jet matched to at least two b-tagged track small-radius jets, one of which contains a muon. Such jets arise naturally in multi-jet production, especially in the case of gluon splitting to bottom quark pairs. Previous measurements suggest that the fraction of such jets containing $b\bar{b}$ in Monte Carlo (MC) simulations cannot be relied on [8]. Therefore, a correction for possible mismodeling of this fraction is derived directly from data. After applying this correction, a comparison between data and MC simulation is performed to examine possible mismodeling of the b-tagging and jet energy, mass and substructure variables.

This note is organized as follows: Section 2 describes the ATLAS detector. Section 3 describes the data and MC simulation samples used in the analysis. Section 4 then presents the physics object selection, while Section 5 describes the event selection based on such physics objects. The flavor fraction correction used to improve the MC simulation predictions of the $b\bar{b}$ fraction is presented in Section 6. Finally, the comparisons between data and MC simulation and validation results for b-tagging and jet performance can be found in Section 7.

2 The ATLAS detector

The ATLAS experiment [1] at the LHC is a multi-purpose particle detector with a forward-backward symmetric cylindrical geometry and a near 4π coverage in solid angle.[1] It consists of an inner tracking detector

[1] ATLAS uses a right-handed coordinate system with its origin at the nominal interaction point (IP) in the centre of the detector and the z-axis along the beam pipe. The x-axis points from the IP to the centre of the LHC ring, and the y-axis points

surrounded by a thin superconducting solenoid providing a 2 T axial magnetic field, electromagnetic and hadron calorimeters, and a muon spectrometer. The inner tracking detector covers the pseudorapidity range $|\eta| < 2.5$. It consists of silicon pixel, silicon micro-strip, and transition radiation tracking detectors. Lead/liquid-argon sampling calorimeters provide electromagnetic energy measurements with high granularity for $|\eta| < 3.2$. A hadronic (iron/scintillator-tile) calorimeter covers the central pseudorapidity range ($|\eta| < 1.7$). The end-cap and forward regions are instrumented with liquid argon calorimeters for both electomagnetic and hadronic energy measurements up to $|\eta| = 4.9$. The muon spectrometer surrounds the calorimeters and is based on three large air-core toroid superconducting magnets with eight coils each. Its bending power is in the range from 2.0 to 7.5 T m. It includes a system of precision tracking chambers ($|\eta| < 2.7$) and fast detectors for triggering ($|\eta| < 2.4$). A three-level trigger system is used to select events. The first-level trigger is implemented in hardware and uses a subset of the detector information, while software-level selection follows. In 2012 data taking the first-level reduced the accepted rate to at most 75 kHz and two software-based trigger levels together reduced the accepted event rate to 400 Hz.

3 Data and Monte Carlo Samples

The data used in this analysis correspond to 20.3 fb^{-1} of good quality 8 TeV pp collision data collected with the ATLAS detector during 2012. The average number of interactions per pp bunch crossing, $\langle\mu\rangle$, was approximately 20.

MC simulation samples of inclusive jet production were produced with Pythia 8.165 [9] with the AU2 [10] tune and the CT10 [11] PDF set and used for comparison with data and to validate the flavor fraction fitting procedure. Additionally, Herwig++ 2.6.3 [12] inclusive jet samples with Jimmy [13] for the underlying event modeling and with the EE3 tune [14] and CTEQ6L1 [15] PDF set were used for additional generator dependence cross-checks.

Several event-level weightings were applied to the MC simulation samples to better reproduce the data. The samples were weighted to have the same μ distribution as the data. In order to correct the trigger efficiency the events used in the analysis were reweighted to reproduce the p_{T} and η distribution of the highest p_{T} jet in the event as described in Section 5. Additionally, jet flavor fractions corrections are also applied as described in Section 6.

4 Object selection, association, and flavor labeling

The selection, the matching criteria or association, and the determination of the heavy flavor content of physics objects for this analysis are described below.

Calorimeter Jets: The standard inputs to calorimeter jet reconstruction in ATLAS are topological clusters of calorimeter cell energy depositions [16]. The clusters are considered massless, and are calibrated using the local cluster weight method [17]. In this analysis, calorimeter jets reconstructed using FastJet v2.4.2.5 [18, 19] with the anti-k_t algorithm [20] are used. Calorimeter jets reconstructed with a distance

upwards. Cylindrical coordinates (r, ϕ) are used in the transverse plane, ϕ being the azimuthal angle around the z-axis. The pseudorapidity is defined in terms of the polar angle θ as $\eta = -\ln\tan(\theta/2)$. Angular distance is measured in units of $\Delta R \equiv \sqrt{(\Delta\eta)^2 + (\Delta\phi)^2}$.

parameter of $R = 0.4$ are used to trigger the event and those reconstructed with R=1.0, large-R jets, are used for studying the $g \to b\bar{b}$ system.

For both data and MC, $R = 0.4$ jets are then calibrated using p_{T}- and η- dependent calibration factors based on MC simulations [21]. Afterwards, a residual calibration derived from several in situ techniques is applied to data. Only $R = 0.4$ jets with $p_{\mathrm{T}} > 20$ GeV and $|\eta| < 2.5$ are used. Jets with significant contributions from pile-up interactions [22] are removed by requiring that jets with $p_{\mathrm{T}} < 50$ GeV and $|\eta| < 2.4$ have at least 50% of the p_{T} sum of tracks matched to the jet belonging to tracks originating from the hard-scatter vertex[2].

The trimming algorithm [23] adopted by ATLAS as the standard grooming procedure is applied to the anti-k_t jets with $R = 1.0$, in order to discard the softer components of the jet including contributions from pile-up and underlying event. For trimming, k_t subjets with $R_{\mathrm{sub}} = 0.3$ are used with $f_{\mathrm{cut}} = 0.05$. After this grooming procedure, the jet energy and mass for both data and MC simulated events are calibrated using particle-level correction factors derived from simulation [24]. These calibration factors correct the mean of the mass and energy distribution and set the mass and energy scale of the jets, and are referred to as the jet mass scale (JMS) and jet energy scale (JES), respectively. The calibration procedure is described in detail in Ref. [25]. Only large-R jets with $p_{\mathrm{T}} > 200$ GeV and pseudorapidity $|\eta| < 2.0$ are considered in this analysis.

The systematic uncertainties on the large-R JES and JMS have been derived using an inclusive multi-jet selection. They have been derived using in situ methods by comparing the measured calorimeter jet energy, mass and substructure variables to the same quantities for large radius jets built from tracks [26] in both data and simulation, using the double ratio:

$$\langle r^{X}_{\mathrm{trk}} \rangle_{\mathrm{data}} / \langle r^{X}_{\mathrm{trk}} \rangle_{\mathrm{MC}}, \tag{1}$$

where $r^{X}_{\mathrm{trk}} = X^{\mathrm{calo}}/X^{\mathrm{trk}}$ and X denotes the jet mass, energy or substructure variable. Large-R track jets geometrically associated to the calorimeter jets are used as reference objects, since tracks from charged hadrons are well-measured and are independent of the calorimeter. The inner detector and the calorimeter have largely uncorrelated instrumental systematic effects, and so a comparison of variables such as jet mass and energy between the two systems allows a separation of physics and detector effects. Also, the use of tracks reduces the impact of pile-up since tracks are required to come from the hard scattering vertex. This technique achieves a precision of around 3-7% in the central detector region, which is dominated by systematic uncertainties arising from the inner-detector tracking efficiency and MC simulation modeling uncertainties of the charged and neutral components of jets.

Track Jets: Track jets are reconstructed from inner detector tracks using the anti-k_t algorithm with a distance parameters of $R = 0.2$ [27]. The tracks are required to have:

- $p_{\mathrm{T}} > 0.5$ GeV and $|\eta| < 2.5$;
- at least 6 hits in the silicon detectors (pixel detector + silicon microstrip detector);
- a tight match to the hard-scatter vertex by requiring that the track transverse and longitudinal impact parameter with respect to the hard-scatter vertex, d_0 and z_0 respectively, satisfy $|d_0| < 1.5$ mm and $|z_0 \sin(\theta)| < 1.5$ mm, where θ is the track polar angle.

[2] The hard-scatter vertex is the reconstructed collision vertex with the highest sum p^2_{T} of tracks used to form the vertex.

These requirements greatly reduce the number of tracks from pile-up vertices whilst being highly efficient for tracks from the hard-scatter vertex. Only track jets with $p_{\mathrm{T}} > 10$ GeV, $|\eta| < 2.5$, and with at least two tracks are used for the analysis. The b-tagging efficiency of track jets for jets containing true b-hadrons was calibrated using Run 1 $t\bar{t}$ candidate data events. The calibration for charm and light-flavor jets is taken from the calibration performed with $R = 0.4$ calorimeter jets with a p_{T} scaling to account for the difference in track jet and calorimeter jet p_{T}, and with additional uncertainties to account for possible differences between track jet and calorimeter jet b-tagging.

Muons: Muons are reconstructed from a combination of measurements from the inner detector and the muon spectrometer. Muons selected for this analysis are required to have $p_{\mathrm{T}} > 5$ GeV and $|\eta| < 2.4$, and to be consistent with the primary vertex by requiring $|d_0| < 2$ mm and $|z_0 \sin(\theta)| < 2$ mm. The reconstruction efficiency ranges between 95-99% in most of the detector, except for $1.0 < |\eta| < 1.3$ where it is around 85% [28].

Jet to Jet Association: In events with a dense hadronic environment, there can often be an ambiguity when matching track jets to calorimeter jets. The track jet association to large-R jets is performed using ghost-association [24, 29, 30], which provides a robust matching procedure that makes use of the catchment area of the jet [29]. As a result, matching to jets with irregular boundaries can be achieved in a less ambiguous way than a simple geometric (i.e. ΔR between objects) matching. In this procedure, the "ghosts" are the track jet 4-vectors in the event, with the track jet p_{T} set to an infinitesimal amount, essentially only retaining the direction of the track jets. This ensures that jet reconstruction is not altered by the ghosts when the calorimeter clusters plus ghosts are reclustered. The reclustering is then performed using the anti-k_t algorithm with $R = 1.0$. The calorimeter jets after reclustering are identical to the ungroomed parents of the trimmed jets used in this analysis, with the addition of the associated track jets retained as constituents. In this analysis, track jets ghost-associated to the large-R jet refer to track jets found this way within the catchment area of the ungroomed parent jet, but the kinematics of the large-R jet are still measured using the trimmed jet.

Jet to Muon Association: Semi-leptonic decays of the b-hadrons can be identified through a jet to muon association. Muon association to track jets is done by geometrical matching, i.e. the muon is required to be within $\Delta R = 0.2$ of the track jet direction.

Jet Flavor Labeling: The labeling of the flavor of the track jets in simulation is done by geometrically matching the jet with generator-level hadrons: if a weakly decaying b-hadron is found within $\Delta R < 0.3$ of the jet direction, the jet is labeled as a b-jet. In the case that the b-hadron could match more than one jet, only the closest jet is labeled as a b-jet. If no b-hadron is found, the procedure is repeated for weakly decaying c-hadrons to label b-jets. A jet for which no such association can be made is labeled as a light-flavor or L-jet.

The large-R jet's flavor composition is denoted by the flavor composition of the selected track jets within the jet. As this analysis will primarily select two track jets to examine within the large-R jet, the large-R jet flavor will be denoted by the two flavors of the track jets. For example, a large-R jet with two selected b-labeled track jets will be labeled a "BB" large-R jet.

***b*-jet Identification:** Several algorithms to identify b-jets have been developed based on the lifetime decay properties of b-hadrons [4]. Tracks that are associated to the jets and that pass basic quality requirements are used as inputs to the algorithms. The algorithms use relatively simple track impact parameter (IP3D) and secondary vertex (SV1) information, or, in the case of the more refined JetFitter algorithm, exploit the topology of weak b- and c-hadron decays using a Kalman filter to search for a common line connecting the primary vertex to beauty and charm decay vertices. The tagger used in this analysis, MV1, combines

the output of these taggers in a neural network for improved b-jet efficiency and c-jet and light-flavor jet rejection.

The efficiency of the b-tagging algorithm is calibrated in data by comparing the measured tagging efficiencies to those in the MC simulation and deriving correction factors, or "scale factors", as a function of p_{T} and η for the MC simulation [4]. The calibrations are typically performed in the case when fixed thresholds are applied to the tag weights computed by the b-tagging algorithms. These fixed thresholds or "working points" (WP) are tuned to obtain specified b-jet efficiencies based on the inclusive p_{T} and η spectra of jets from an inclusive $t\bar{t}$ sample. In this note, the working point used to tag a jet as originating from a b-quark is the 70% WP, which has typical light-flavor jet and c-jet mistag rates of 0.01 and 0.2, respectively. The uncertainty on the calibration scale factors of the b-tagging efficiency on track jets is approximately 3%-8% for track jets with $p_{\mathrm{T}} < 250$ GeV. Above this track jet p_{T} sufficient data is not available for calibration. Therefore, extrapolation uncertainties, evaluated as the effect of varying detector related parameters on the tagging efficiencies in simulation, are added.

5 Event Selection

Events are selected using single jet triggers with varying jet p_{T} thresholds above 80 GeV as measured by the trigger jet reconstruction. All triggers with trigger jet $p_{\mathrm{T}} < 360$ GeV are prescaled so as not to overwhelm the trigger data output rate. Single jet triggers with trigger jet $p_{\mathrm{T}} \geq 360$ GeV are not prescaled, and are fully efficient for $R = 0.4$ jets with offline jet $p_T > 430$ GeV. Events must have been recorded by the highest p_{T} trigger that is fully efficient for the highest p_{T} $R = 0.4$ offline jet in the event. The leading p_{T} $R = 0.4$ offline jet is called the triggering jet, j_{trig}. No explicit matching is made of these jets to the trigger system jet that fired the trigger.

Selected events are required to have at least one large-R jet with $p_{\mathrm{T}} > 200$ GeVand $|\eta| < 2.0$. Additionally this jet must have at least two ghost associated $R = 0.2$ track jets. In order to enrich the event sample in jets containing b-hadrons, it is required that at least one of the ghost associated track jets be matched to a muon. The highest p_{T} track jet matched to a muon is called the muon-tagged jet. The next leading p_{T} ghost-associated track jet is called the non-muon jet. This requirement selects semi-leptonic b-hadron decays. The highest p_{T} large-R jet passing these criteria is selected as the gluon jet candidate. In addition, the event must satisfy $\Delta R(j_{\mathrm{trig}}, j_{\mu}^{\mathrm{trk}}) > 1.5$ where j_{μ}^{trk} is the muon matched track jet found within the large-R jet. This requirement ensures that the triggering jet and the gluon candidate jet are well separated, and thus that the trigger requirement is independent of the gluon candidate selection. Finally, the b-tagged sample used in the analysis is defined by applying b-tagging to the two $R = 0.2$ track jets ghost associated to the large-R jet.

As the trigger prescaling shapes the offline jet p_{T} spectrum, the spectrum of j_{trig} in MC simulation is weighted to match the observed spectrum in the data. Additionally, there is an observed difference of the η spectrum of j_{trig} between data and MC simulation, so a reweighting is applied to the MC simulation in this variable.

6 Flavor Fraction Corrections

In order to study the performance of the tagging algorithm and modeling of jet properties, discrepancies arising from differences between data and MC simulation in the flavor composition of the large-R jet must be factorized out of the comparison. Therefore, the flavor fractions of the sample are determined directly from the data by fitting a distribution sensitive to the relative composition of the different flavors of jets before using jet flavor tagging. Flavor fraction corrections are applied before doing the data to MC simulation comparison presented in Section 7. The following describes the flavor fraction determination.

6.1 S_{d_0} as Discriminant Variable

The long decay length of heavy flavor hadrons makes the signed significance of impact parameter s_{d_0} of tracks associated to a jet a good discriminating variable. The s_{d_0} of a track is defined as

$$s_{d_0} = \frac{d_0}{\sigma(d_0)} \cdot s_j \tag{2}$$

where d_0 is the track transverse impact parameter with respect to the primary vertex, $\sigma(d_0)$ is the uncertainty on the d_0 measurement, and s_j is the sign of d_0 with respect to the jet axis, depending on whether the track crosses the jet axis in front or behind the primary vertex.

For a given track jet, only the track with the highest absolute s_{d_0} is considered. This s_{d_0} value is denoted as S_{d_0}. Templates are constructed from MC simulation for large-R jets using the two S_{d_0} values for the two ghost associated track jets. The data are fitted simultaneously to the S_{d_0} distribution of both track jets in order to derive the flavor fractions of the track jet pairs. The MC simulation is then corrected to the observed fit fraction when doing comparisons of the b-tagging and jet properties.

6.2 Maximum Likelihood Estimation

A k flavor pair component template fit is carried out by maximizing a binned likelihood function defined as $\mathcal{L} = \prod_{i=1}^{n} p(y_i|\vec{\theta})$, where $\vec{\theta} \in \mathbb{R}^k$ denotes the number of events from each flavor pair component, n is the number of bins being fitted and y_i is the number of data events in bin i. k may take a maximum value of 9 as there are 9 ordered flavor pairs, however it is reduced to 5 for the purposes of this fit, as described in Section 6.3. It is assumed that $p(y_i|\vec{\theta})$ is a Poisson distribution:

$$p(y_i|\vec{\theta}) = \frac{\exp\left(-\vec{\theta}\cdot\vec{x_i}\right)(\vec{\theta}\cdot\vec{x}_i)^{y_i}}{y_i!}, \tag{3}$$

where $\vec{x_i} = (x_{i1}..., x_{ij}..., x_{ik}) \in \mathbb{R}^k$ is a vector, and each component denotes the i^{th} bin value in the normalized templates for the j^{th} flavor pair (bb, cc, c-light and etc.). Flavor fractions are determined by finding the $\vec{\theta}$ that maximizes $\mathcal{L}$. The determination of the statistical uncertainties on the fitted parameters is carried out by taking Poisson fluctuations of the data 1000 times and refitting the resulting pseudo-experiment data with the templates. The standard deviation of these fits results is taken as the fit uncertainty.

6.3 S_{d_0} Templates

The flavor content of the two track jets associated to the large-R jets is correlated and should not be treated independently. Therefore, the fit is done in pairs of the track jet S_{d_0}. However, the jets' S_{d_0} values are not correlated, and a Naive Bayes classifier approximation method can be used: the flavor fractions are estimated by fitting simultaneously the 1-dimensional S_{d_0} distributions of the muon tagged jet and the other tagged jet using templates derived from all of the possible two-jet flavor pair combinations. Templates for the muon tagged and non-muon track jets are derived separately.

There are in total nine different ordered flavor pairs: BB, BL, BC, CB, CL, CC, LB, LC and LL such that the first flavor is that of the track jet with a muon and the second is that of the other track jet. In the MC simulations, the fractions of BC, CB, LC and LB are all less than 1% of the total. These components can not be fit accurately due to their small size. Therefore, they are merged with the most similar templates of large flavor fractions BL, CL and LL. The metric used for determining the similarity between two distributions is:

$$S = \frac{1}{2}\int \frac{(p_1(x) - p_2(x))^2}{p_1(x) + p_2(x)}\mathrm{d}x \tag{4}$$

where $p_1(x)$ and $p_2(x)$ are two different distributions. The following templates are merged using this metric: the BC template with the BL template; the LC and LB templates with the LL template; and the CB template with the CL template. Figure 1 shows the templates used in the fit. It can be seen that on average the muon jet templates are broader than the non-muon jet templates, and that the BL component in the non-muon jet template shows a slightly higher positive tail than the CC, CL and LL templates. This can be caused by contamination of the b-hadron tracks in the light-flavor jet or from mislabeling of the jet as light.

The fitting procedure is validated through several tests detailed below.

- **MC simulation closure:** the MC simulation closure is tested by randomly dividing the MC simulation sample into two subsets and using the templates derived from one to fit the other. The fitted flavor fractions are found to agree well with the truth values. The largest discrepancy is 1.5σ in the "CL" component which is less than 1% of the event sample after b-tagging.
- **Fit linearity:** a fit linearity test is performed by varying the BB fraction from 0.5% up to 13.5% in steps of 1.0% and check if the fit is stable for different BB fractions, especially if the fit will fluctuate to zero when the BB fraction is low. The fit is stable down to a BB fraction of approximately 1%. Below this value the statistical uncertainty is comparable to the fit central value.
- **C and L component degeneracy:** Because the CC and CL components are small and similar to the LL components, the quality of the fit is also tested with these components merged with the LL templates. The results are consistent with the 5-component fit results.
- **Impact of tracking systematic uncertainties on S_{d_0} resolution:** Studies of the track impact parameter resolution show a difference between data and MC simulation [31]. To evaluate how these differences would affect the template shapes a smearing of the core impact-parameter resolution which reproduces the data resolution is also applied to the S_{d_0} distribution. It is applied to the d_0 distribution but not to the covariance matrix of the track fit which gives the impact parameter uncertainty. The smeared templates were used in the fit, and the resulting flavor fractions were applied to the MC simulation. The BB fraction changed by an absolute 0.03% using the smeared templates. No smearing was applied outside of the core of the distribution, but good agreement is seen between the data and the template fits in Figure 2 and 3.

- **Correlations between S_{d_0} and MV1:** Biases in the fit due to correlations in the b-tagging discriminant value of the track jets which pass the b-tagging cut with the S_{d_0} value are investigated. The sample is divided into two subsets which are labeled as pseudo-data and MC simulation. The BB events which pass the b-tagging cut in the pseudo-data subset are reweighted by a factor of 2 or $\frac{1}{2}$ and then fitted by the templates derived from the MC simulation subset. These factors are correspond to an effective change of 10% in the single b-tagging efficiency. Reweighting by a factor of 2, the pseudo data BB fraction is 12.2% ± 0.1%, while the fitted BB fraction is 12.6% ± 0.5%. Reweighting by a factor of $\frac{1}{2}$, the pseudo data BB fraction is 6.6% ± 0.1%, while the fitted BB fraction is 6.7% ± 0.4%. No bias is seen within the uncertainties reported by the fits. These results show that the correlation between S_{d_0} and MV1 are small.

These studies show that the fit is a robust method of determining the flavor fractions. Their impact on the fit performance is negligible and therefore no additional systematic uncertainties due to these effects were taken into account.

6.4 Fit Results

The flavor fractions vary significantly as a function of the p_{T} of track jets. Therefore, the simultaneous fit to the S_{d_0} distributions of the muon and non-muon track jet is carried out in p_{T} bins of the two track jets. The sample is divided into three regions based on the muon track jet p_{T} ($p_{\mathrm{T},1}$: <70 GeV, 70-150 GeV, >150 GeV), each of which is then divided into four regions based on p_{T} of the other track jet ($p_{\mathrm{T},2}$: <20 GeV, 20-50 GeV, 50-80 GeV, >80 GeV). Differences between the fitted and nominal MC simulation predicted value of up to 50% in the BB flavor fraction are found for individual bins of the small radius jet p_{T}. Figures 2 and 3 show two examples of the simultaneous fit to the S_{d_0} distributions. A 1σ variation of the flavor fraction fit is taken as uncertainty on the data/MC ratio. In general, the MC simulation underestimates the fraction of BB jets, and overestimates the contribution of CL, although the specific corrections vary bin-by-bin. Figure 4 shows a comparison between the flavor fractions predicted by MC simulation and the simultaneous fit to S_{d_0} distributions as a function of the large-R jet p_{T}. Only the LL, BL and BB components are shown for clarity. The BB fraction is 12% in the lowest p_{T} bin, and decreases to 3% in the highest p_{T} bins. The LL and BL fractions show a flat or decreasing fraction at low p_{T} where the trigger prescales sculpt the underlying p_{T} distribution. Above Clear differences between the default MC simulation and data-derived flavor fraction can be seen, especially when the large-R jet has $p_{\mathrm{T}} < 500$ GeV, further confirming the need for this correction.

7 Results

After correcting for the observed flavor-pair fractions, the agreement between data and MC simulation is evaluated in the selected event sample before and after b-tagging is applied to the small-radius track jets.

7.1 b-tagged jet properties

As the flavor fractions are corrected in the MC simulation, deviations between the data and predictions after b-tagging can be attributed to a difference between data and MC simulation in the dependence of

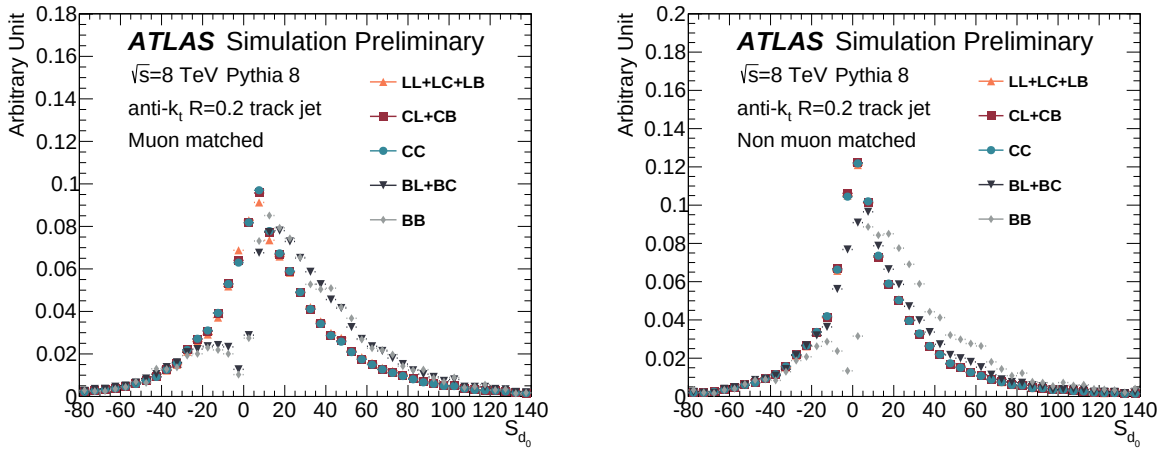

Figure 1: The S_{d_0} distributions for muon (left) and non-muon jets (right). The double flavor labels in the plots denote the flavor of the jet pair, with the muon jet given first.

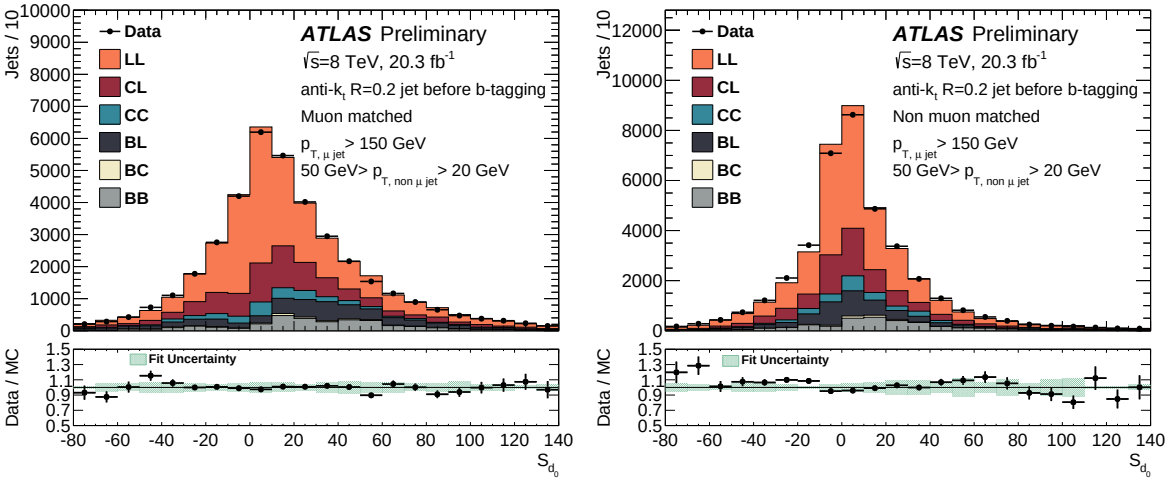

Figure 2: S_{d_0} distributions in data and simulation, after the simultaneous fit in bin of muon jet p_{T} >150 GeV(left) and non-muon jet 50 GeV> p_{T} >20 GeV(right). The flavor components shown include both combinations of flavors for the muon and non-muon matched jets. The green band indicates 1σ variation of flavor fraction fit.

the *b*-tagging performance on the event topology, beyond the scale factors derived for inclusive jets as discussed in Section 4.

After requiring two *b*-tagged small-radius track jets, the ratio of the number of data events to MC simulated events is 0.98 ± 0.01(Stat.) ± 0.10(Syst.) and the BB purity, as estimated from the simulation, is approximately 85%. The MC simulation is normalized to the number of data events prior to *b*-tagging and corrected for the flavor fractions derived in Section 6. It also includes scale factors for the true *b*-tagging efficiency derived from studies of *b*-tagging rates on small-radius track jets in $t\bar{t}$ events. These b-tagging efficiency scale factors were derived using an inclusive sample of b-tagged jets and are applied to muon jets and non-muon jets. The *b*-tagging systematic uncertainty is determined from those studies. Light-flavor and *c*-jets receive no scale factor, but constitute only 10% of the tagged small-radius jets. This level of agreement indicates that on average the MC simulation of the *b*-tagging performance is in

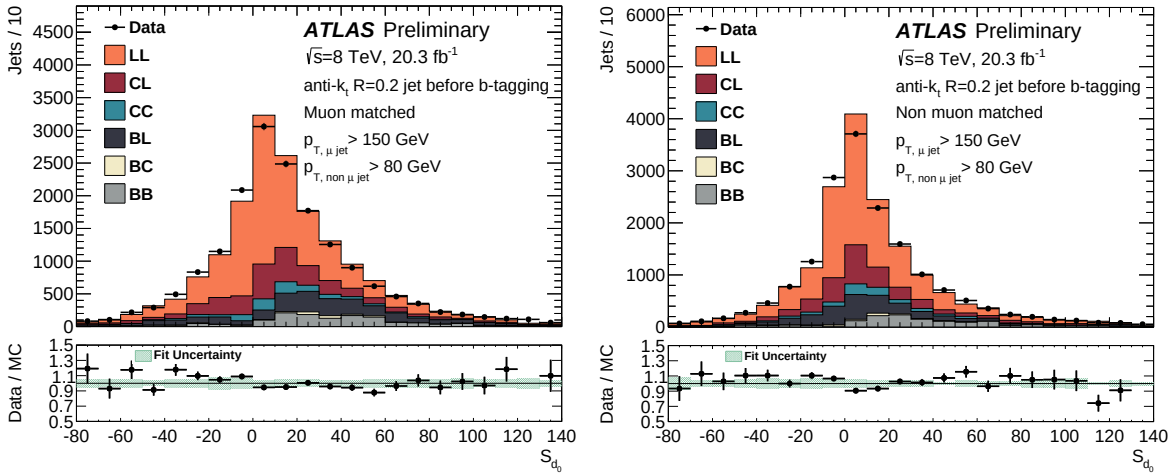

Figure 3: S_{d_0} distributions in data and simulation, after the simultaneous fit in bin of muon jet p_{T} >150 GeV(left) and non-muon jet p_{T} >80 GeV(right). The flavor components shown include both combinations of flavors for the muon and non muon matched jets. The green band indicates 1σ variation of flavor fraction fit.

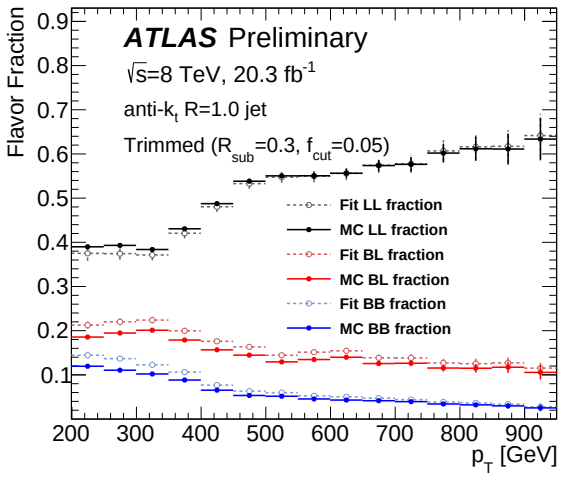

Figure 4: Comparison of major flavor fractions predicted by MC simulation and the simultaneous fit to S_{d_0} distributions in data as a function of the large-R jet p_{T}.

good agreement with the data in the large-R jet topology.

Figure 5 shows the distribution of the ΔR between the two small-radius track jets before and after b-tagging is applied, after the flavor corrections are applied. The ratio of data to MC simulation in the ΔR distribution is consistent with unity within the total systematic uncertainty. It is notable that the same level of agreement is seen even at low values of ΔR in which the jets are not isolated from other jets.

Figure 6 shows the small-radius jet p_{T} distributions for the muon and non-muon jet before and after tagging. After tagging the sample is dominated by b-jets and the MC simulation agrees with the data within the total systematic uncertainty. Figure 7 shows the p_{T} distributions for the muon matched to the muon jet. Before and after tagging the MC simulation agrees with the data within 1σ of the total systematic uncertainty.

Lastly, the double b-tagging rate as a function of the large-R jet p_{T} is shown in Figure 8. Data and MC simulation agree well within the uncertainties, which include both the large-R jet energy scale and b-tagging uncertainties. The uncertainty on the JES of the track jets is small compared to the b-tagging uncertainty and therefore is not included.

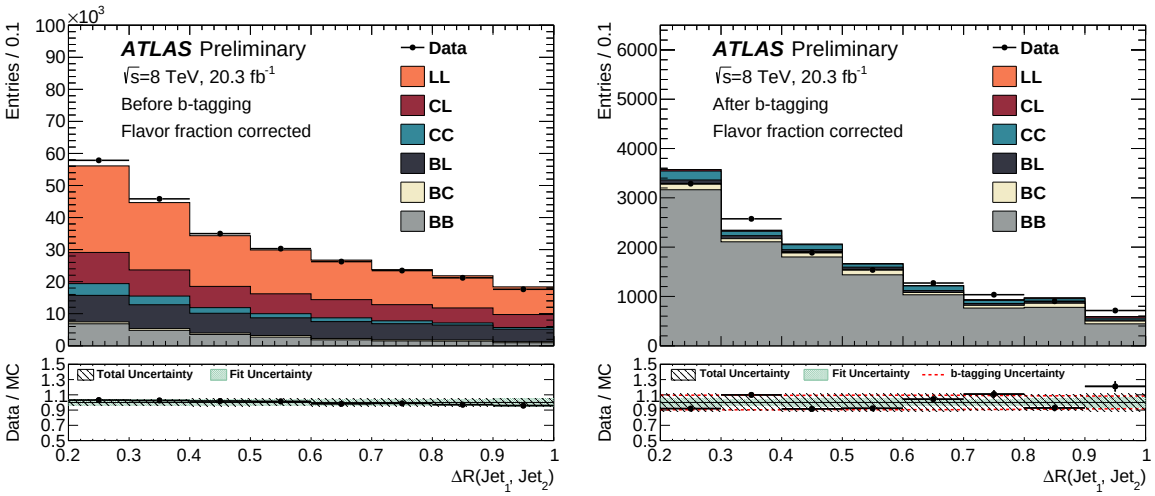

Figure 5: ΔR between the muon-jet and non-muon jet before (left) and after b-tagging (right). b-tagging scale factors and the flavor fraction correction have been applied. The total systematic uncertainty, indicated by the hashed band, includes a 1σ variation on the b-tagging scale factor, the large-R jet JES and the flavor fraction fit. The green band indicates 1σ variation of flavor fraction fit only.

7.2 Large-R jet properties

The $g \to b\bar{b}$ enriched topology is one of the few topologies which allows the modeling of jet variables used to identify boosted Higgs bosons decaying to $b\bar{b}$ pairs to be studied within an environment enriched in heavy-flavor. These are the jet mass and jet substructure variables. Only a subset of substructure variables, computed using the constituents of the large-R jet, were found to be the most discriminant for the purpose of boosted Higgs-jet tagging in recent studies aimed at Run-2 of the LHC [7]:

- $D_2^{(\beta=1)}$ [32]: a variable based on a ratio of the jet two- and three-point energy correction functions, which are constructed from the energies and pair-wise angles of particles within a jet. It is optimized for the identification of boosted two-prong jets.

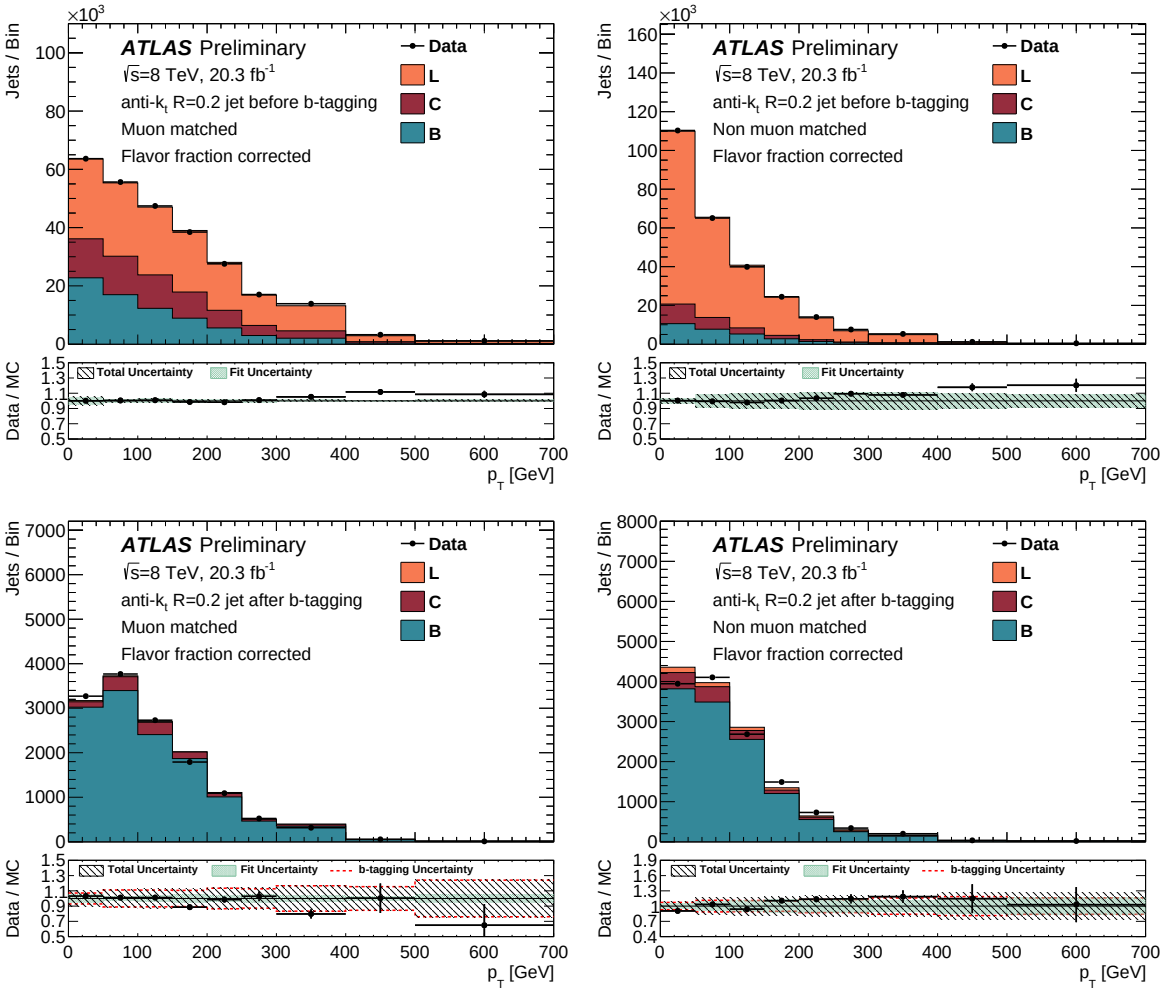

Figure 6: p_{T} of the muon-jet (left) and non-muon jet (right) before (top) and after (bottom) b-tagging. b-tagging scale factors and the flavor fraction correction have been applied. The total systematic uncertainty, indicated by the hashed band, includes a 1σ variation on the b-tagging scale factor, the large-R jet JES and the flavor fraction fit. The green band indicates 1σ variation of flavor fraction fit only.

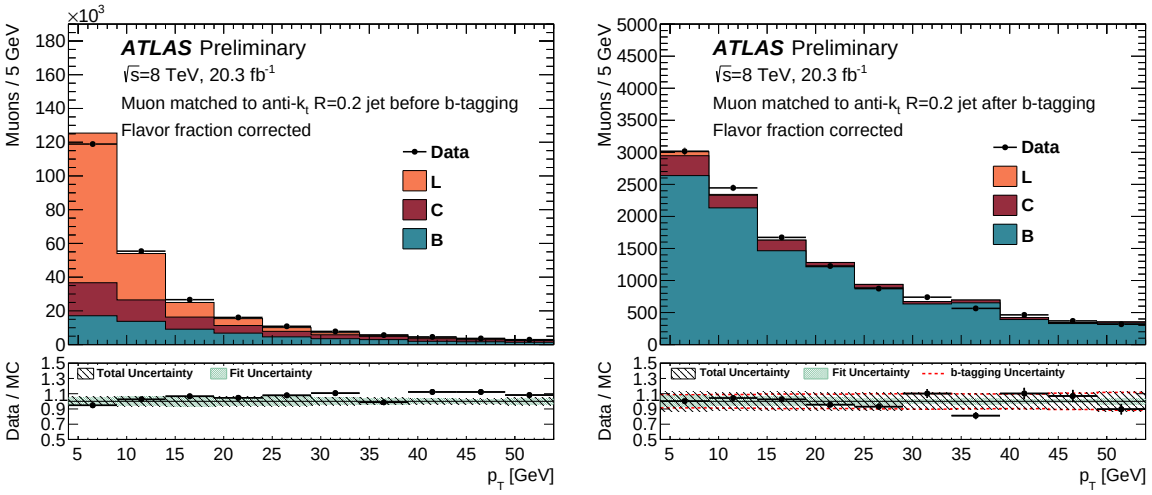

Figure 7: p_{T} of the muon before (left) and after (right) b-tagging. b-tagging scale factors and the flavor fraction correction have been applied. The total systematic uncertainty, indicated by the hashed band, includes a 1σ variation on the b-tagging scale factor, the large-R jet JES and the flavor fraction fit. The green band indicates 1σ variation of flavor fraction fit only.

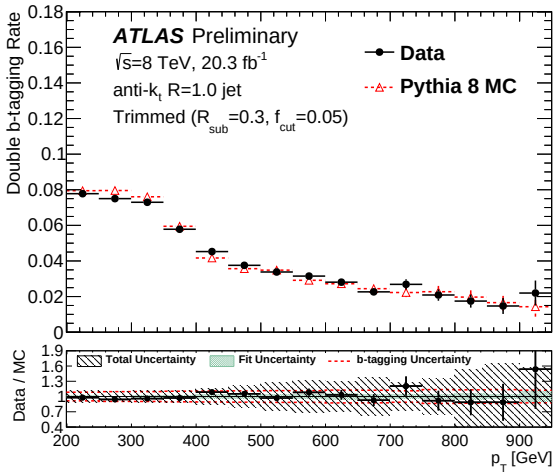

Figure 8: Comparison of data and MC simulation double b-tagging rate as a function of the large-R jet p_{T}. The error bars include statistical uncertainties, as well as the large-R jet energy scale uncertainty and b-tagging scale factor uncertainties.

- τ_{21}^{wta} [33]: a variable based on ratios of the jet shape "N-subjettiness", sensitive to what degree the substructure of a given jet resembles two or one subjets. The "winner takes all" method of defining internal axes is used [34].

A detailed description of these substructure variables can be found in Ref. [25].

Figure 9 shows the agreement between data and MC simulation for the large-R jet p_{T} and mass distributions before and after b-tagging. Figure 10 shows the distribution for $D_2^{(\beta=1)}$ and τ_{21}^{wta} in data and simulation for the large-R jets before and after b-tagging. All the jet properties are well modeled, except the mass distribution which shows small disagreements at low and high values.

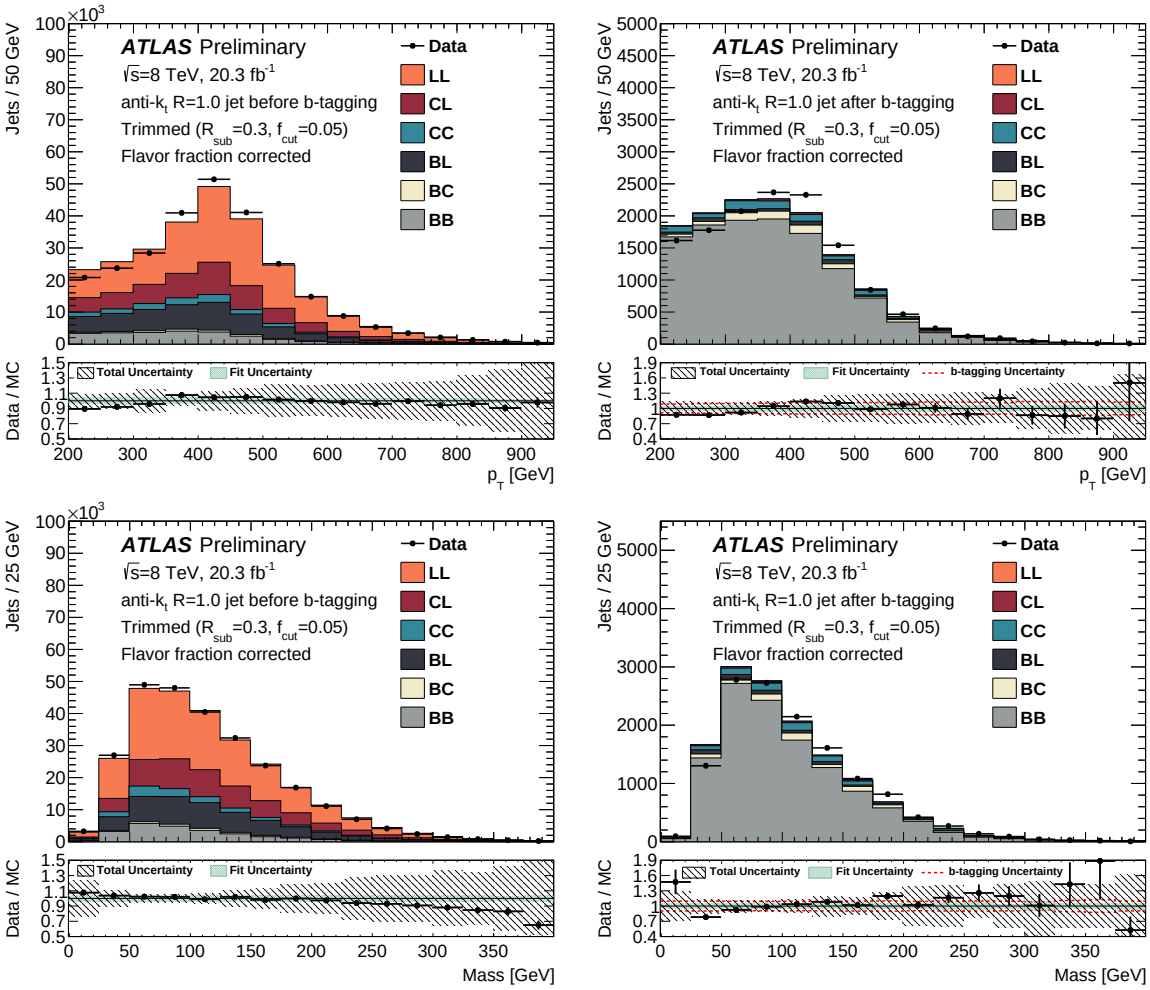

Figure 9: The large-R jet p_{T} (top) and mass (bottom), before (left) and after (right) b-tagging. The flavor fraction correction is applied. The total systematic uncertainty, indicated by the hashed band, includes a 1σ variation on the b-tagging scale factor, the large-R jet energy (top) or mass scale (bottom) and and the flavor fraction fit. The green band indicates 1σ variation of flavor fraction fit only.

The calorimeter-track ratio technique described in Section 4 can be used to study the modeling of the jet mass, energy and substructure scale in the double b-tagged jets sample. Any deviation of the simulation from data not covered by the existing jet scale uncertainties, which have been derived in an inclusive multijet sample, can indicate a need for additional uncertainties in the $b\bar{b}$ topology.

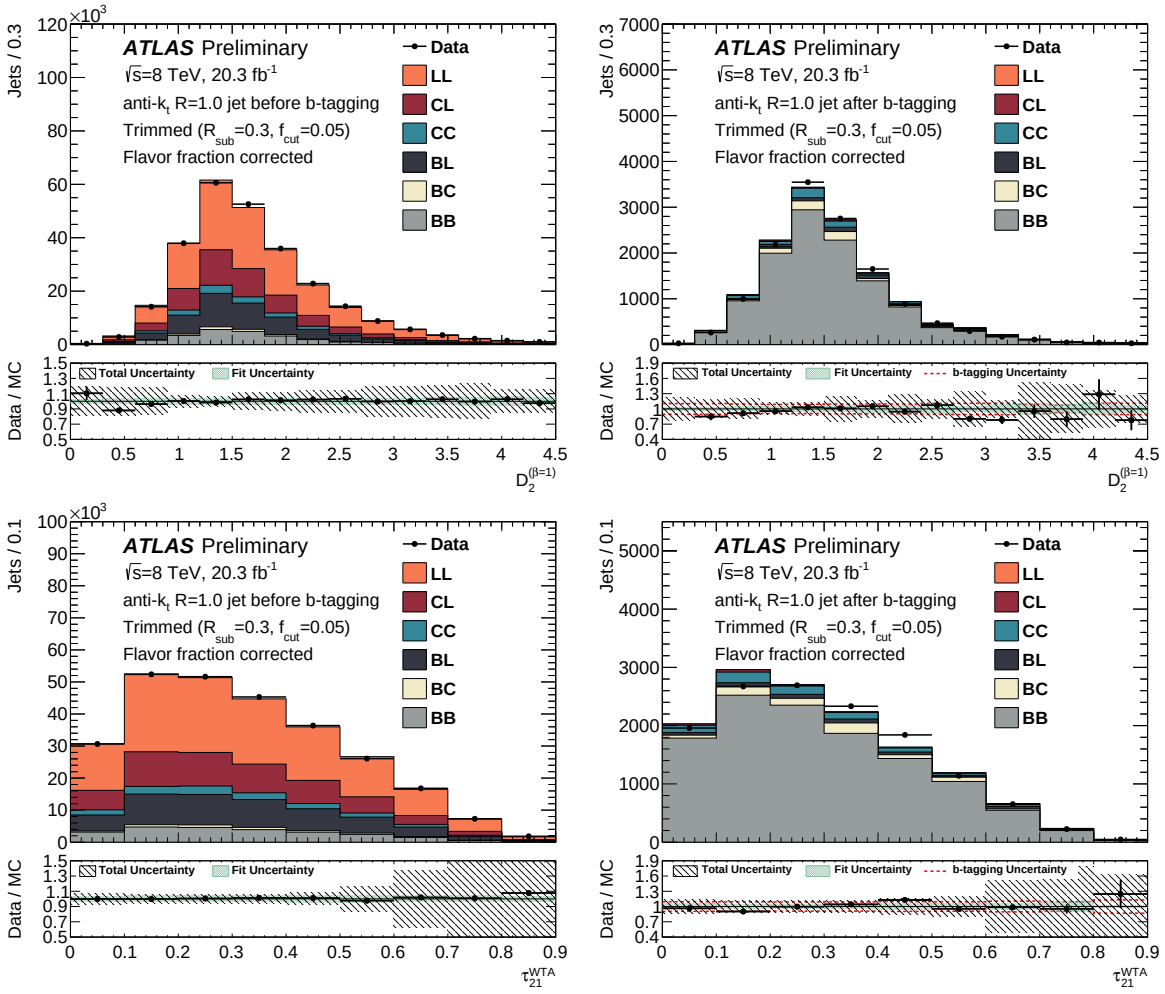

Figure 10: The large-R jet $D_2^{(\beta=1)}$ (top) and τ_{21}^{wta} (bottom), before (left) and after (right) b-tagging. The flavor fraction correction is applied. The total systematic uncertainty, indicated by the hashed band, includes a 1σ variation on the b-tagging scale factor, the large-R jet JES, the $D_2^{(\beta=1)}$ (top) or the τ_{21}^{wta} (bottom) uncertainties and the flavor fraction fit. The green band indicates 1σ variation of flavor fraction fit only.

The calorimeter-track ratio compares the large-R jet property with the same property calculated with large-R track jets that are built using all the tracks ghost-associated to the large-R jet (note that this is different from the small-radius track jets used for b-tagging). The mean values of the single-ratio $X^{\mathrm{calo}}/X^{\mathrm{trk}}$ distributions, which quantifies the potential differences in the variable scale between data and MC simulation, are found to be quite well described.

Figure 11 shows the ratio between data and MC simulation for the mean values of the mass ratio $m^{\mathrm{calo}}/m^{\mathrm{trk}}$ distributions as a function of the ratio of m/p_{T} measured by the reconstructed large-R jet. m/p_{T} is related to the boost of the system as it is proportional to the distance between the decay products of the gluon candidate. The JMS uncertainty is also shown in the figure. The data/MC ratio derived is compatible with the existing JMS uncertainty. Similar results are obtained when comparing the p_{T} and $D_2^{(\beta=1)}$ ratios with their uncertainties, as shown in Figures 12 and 13, respectively.

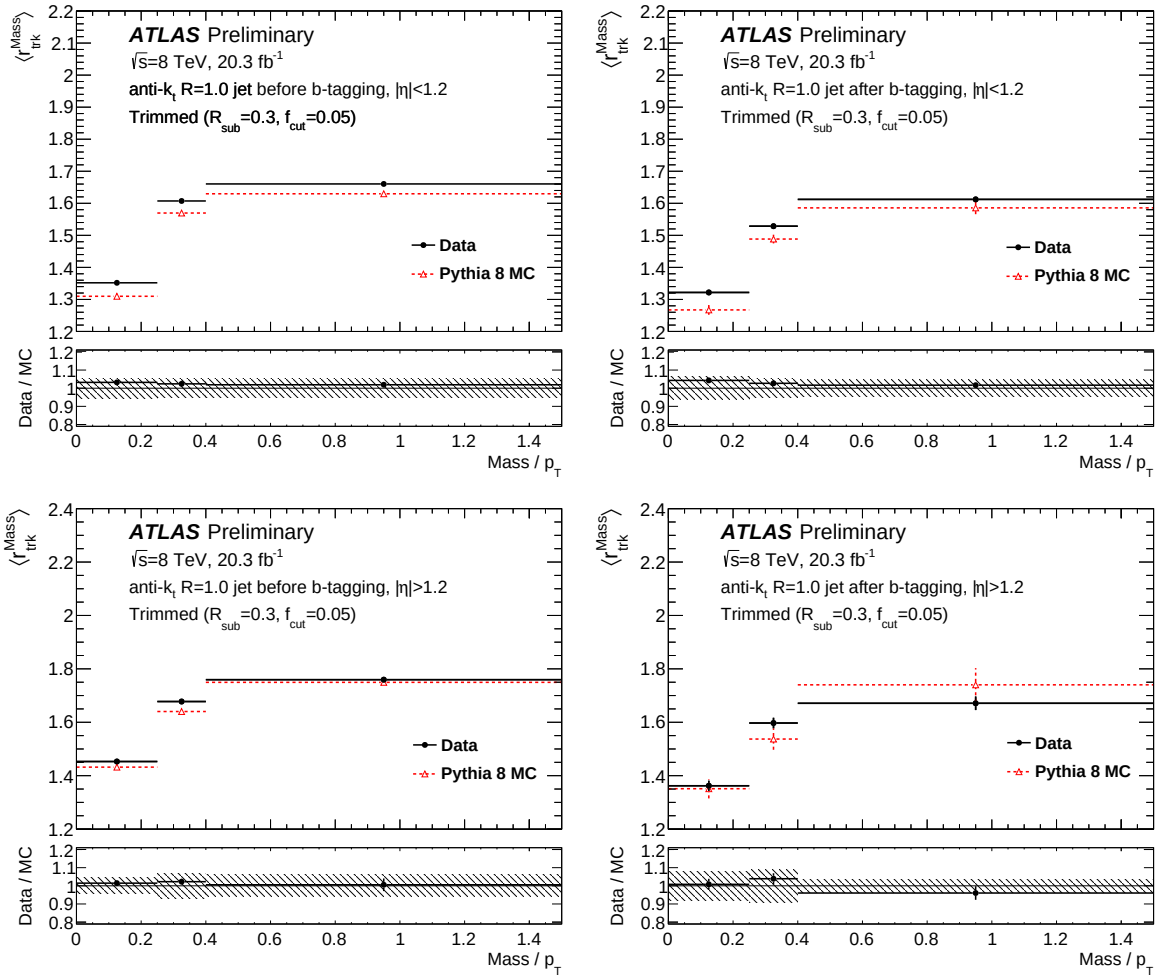

Figure 11: The double ratio $r_{\mathrm{trk}}^{\mathrm{Mass}}$ as a function of the large-R jet mass/p_{T} for central ($|\eta|$ <1.2, top) and forward ($|\eta|$ >1.2, bottom) inclusive (left) and b-tagged (right) jets. In the top panel only statistical uncertainties are shown. In the bottom panel the error bars include the statistical uncertainty, the large-R jet JES and b-tagging uncertainties. The hashed area is the current large-R jet JMS uncertainty.

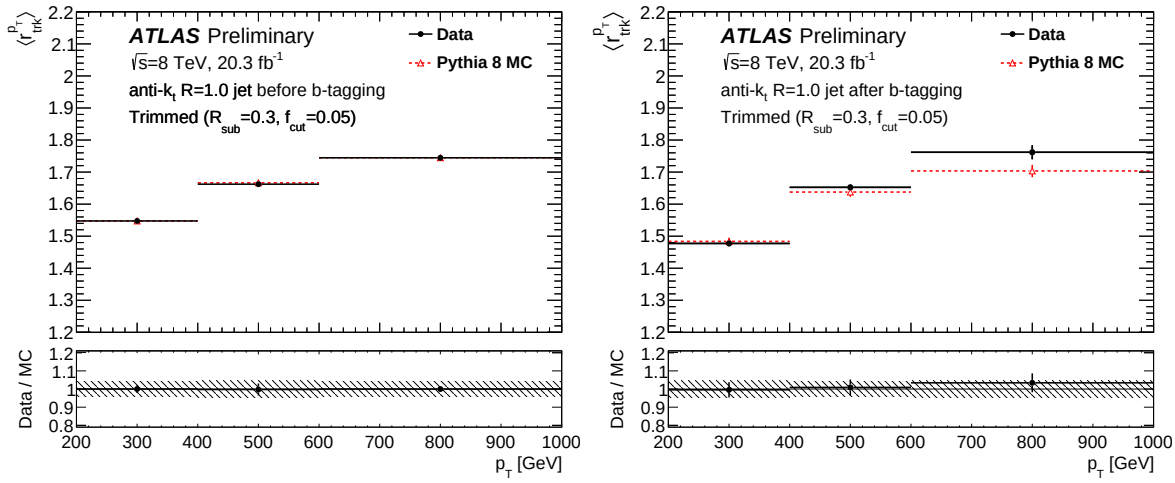

Figure 12: The double ratio $r_{\mathrm{trk}}^{p_{\mathrm{T}}}$ as a function of the large-R jet p_{T} for inclusive (left) and b-tagged (right) jets with $|\eta| < 2.0$. In the top panel only statistical uncertainties are shown. In the bottom panel the error bars include the statistical uncertainty, the generator dependence and b-tagging uncertainties. The hashed area is the current large-R jet JES uncertainty.

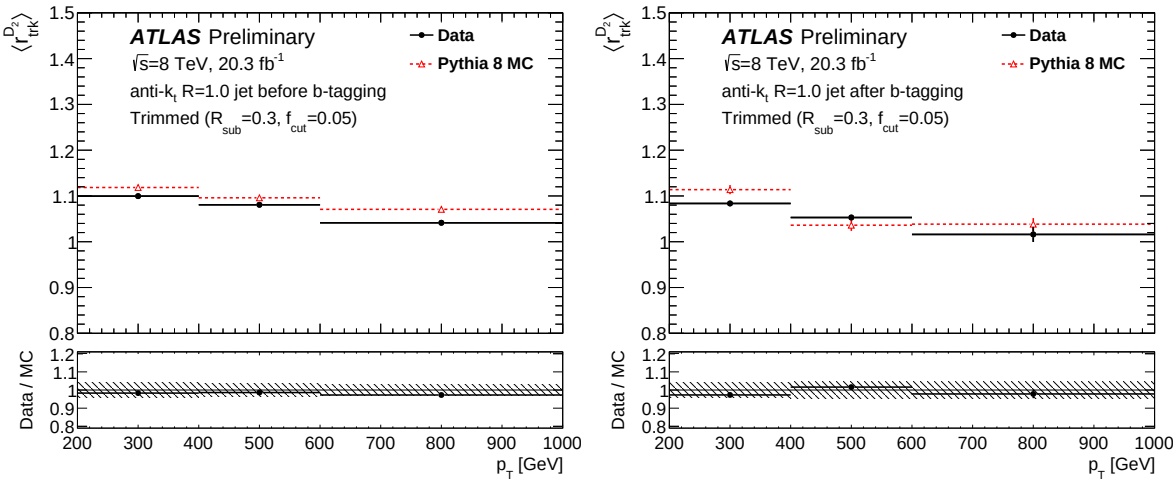

Figure 13: The double ratio $r_{\mathrm{trk}}^{D_2^{(\beta=1)}}$ as a function of the large-R jet p_{T} for inclusive (left) and b-tagged (right) jets with $|\eta| < 2.0$. In the top panel only statistical uncertainties are shown. In the bottom panel the error bars include the statistical uncertainty, the large-R jet JES and b-tagging uncertainties. The hashed area is the current large-R jet $D_2^{(\beta=1)}$ uncertainty.

8 Conclusion

The b-tagging performance and modeling of large-R jet properties in a $g \to bb$ topology with the ATLAS detector at $\sqrt{s} = 8$ TeV has been presented. The analysis is performed in a di-jet sample enriched in double b-tagged jets. The $g \to bb$ candidate jets are reconstructed large-R jets with the anti-k_t, $R = 1.0$ algorithm and trimmed with a subject radius of $R_{\text{sub}} = 0.3$ and $f_{\text{cut}} = 5\%$. They are double b-tagged using associated track jets reconstructed with the anti-k_t, $R = 0.2$ algorithm and the ATLAS b-tagging algorithms. Simultaneous fits of flavor sensitive variables are used to correct possible flavor fraction mismodeling in the MC simulation as a function of p_{T}.

After applying $b-$tagging to the flavor-fraction-corrected sample, good agreement is observed between the data and MC simulation for the $R = 0.2$ track jets kinematic distributions. The jet p_{T} and substructure variables are also found to be well modeled in simulation within uncertainties. Small discrepancies are found in the large-R jet mass distribution. On the other hand, it is found that the differences in large-R jet energy, mass, and substucture scales between data and MC simulation in the boosted $b\bar{b}$ topology are covered by the current jet property systematic uncertainties derived in the inclusive multi-jet sample. Therefore, at present there is no need for additional systematic uncertainties on these variables.

References

[1] ATLAS Collaboration, *The ATLAS Experiment at the CERN Large Hadron Collider*, JINST **3** (2008) S08003.

[2] ATLAS Collaboration, *Search for the $b\bar{b}$ decay of the Standard Model Higgs boson in associated $(W/Z)H$ production with the ATLAS detector*, JHEP **01** (2015) 069, arXiv: 1409.6212 [hep-ex].

[3] ATLAS Collaboration, *Search for Higgs boson pair production in the $b\bar{b}b\bar{b}$ final state from pp collisions at $\sqrt{s} = 8$ TeVwith the ATLAS detector*, Eur. Phys. J. **C75**.9 (2015) 412, arXiv: 1506.00285 [hep-ex].

[4] ATLAS Collaboration, *Performance of b-Jet Identification in the ATLAS Experiment* (2015), arXiv: 1512.01094 [hep-ex].

[5] ATLAS Collaboration, *Calibration of b-tagging using dileptonic top pair events in a combinatorial likelihood approach with the ATLAS experiment*, ATLAS-CONF-2014-004 (2014), URL: http://cdsweb.cern.ch/record/1664335.

[6] ATLAS Collaboration, *Calibration of ATLAS b-tagging algorithms in dense jet environments*, ATLAS-CONF-2016-001 (2016), URL: https://cds.cern.ch/record/2127958.

[7] ATLAS Collaboration, *Expected Performance of Boosted Higgs ($\rightarrow b\bar{b}$) Boson Identification with the ATLAS Detector at $\sqrt{s} = 13$ TeV*, ATL-PHYS-PUB-2015-035 (2015), URL: https://cds.cern.ch/record/2042155.

[8] ATLAS Collaboration, *Measurement of the inclusive and dijet cross-sections of b-jets in pp collisions at $\sqrt{s} = 7$ TeV with the ATLAS detector*, Eur. Phys. J. C **71** (2011) 1846, arXiv: 1109.6833 [hep-ex].

[9] T. Sjostrand, S. Mrenna and P. Z. Skands, *A Brief Introduction to PYTHIA 8.1*, Comput. Phys. Commun. **178** (2008) 852, arXiv: 0710.3820 [hep-ph].

[10] ATLAS Collaboration, *Summary of ATLAS Pythia 8 tunes*, ATL-PHYS-PUB-2012-003 (2012), URL: http://cdsweb.cern.ch/record/1474107.

[11] H.-L. Lai et al., *New parton distributions for collider physics*, Phys. Rev. **D 82** (2010) 074024, arXiv: 1007.2241 [hep-ph].

[12] M. Bahr et al., *Herwig++ Physics and Manual*, Eur. Phys. J. **C 58** (2008) 639, arXiv: 0803.0883 [hep-ph].

[13] J. M. Butterworth, J. R. Forshaw and M. H. Seymour, *Multiparton interactions in photoproduction at HERA*, Z. Phys. C **72** (1996) 637, arXiv: 9601371 [hep-ph].

[14] S. Gieseke, C. Rohr and A. Siodmok, *Colour reconnections in Herwig++*, Eur. Phys. J. **C 72** (2012) 2225, arXiv: 1206.0041 [hep-ph].

[15] P. M. Nadolsky et al., *Implications of CTEQ global analysis for collider observables*, Phys. Rev. **D 78** (2008) 013004, arXiv: 0802.0007 [hep-ph].

[16] W. Lampl et al., *Calorimeter Clustering Algorithms : Description and Performance*, ATL-COM-LARG-2008-003 (2008), URL: http://cdsweb.cern.ch/record/1099735.

[17] ATLAS Collaboration,
Jet energy measurement with the ATLAS detector in proton- proton collisions at $\sqrt{s} = 7$ *TeV*,
Eur.Phys.J. **C73** (2013) 2304, arXiv: 1112.6426 [hep-ex].

[18] M. Cacciari and G. P. Salam, *Dispelling the* N^3 *myth for the* k_t *jet-finder*,
Phys. Lett. **B641** (2006) 057, arXiv: hep-ph/0512210.

[19] M. Cacciari, G. P. Salam and G. Soyez, *FastJet User Manual*, Eur. Phys. J. **C 72** (2012) 1896,
arXiv: 1111.6097 [hep-ph].

[20] M. Cacciari, G. P. Salam and G. Soyez, *The anti-*k_t *jet clustering algorithm*, JHEP **04** (2008) 063,
arXiv: 0802.1189 [hep-ph].

[21] ATLAS Collaboration, *Jet energy measurement and its systematic uncertainty in proton-proton collisions at* $\sqrt{s} = 7$ *TeV with the ATLAS detector*, Eur. Phys. J. **C75** (2015) 17,
arXiv: 1406.0076 [hep-ex].

[22] ATLAS Collaboration, *Pile-up subtraction and suppression for jets in ATLAS*,
ATLAS-CONF-2013-083 (2013), URL: http://cds.cern.ch/record/1570994.

[23] D. Krohn, J. Thaler and L.-T. Wang, *Jet Trimming*, JHEP **02** (2010) 084,
arXiv: 0912.1342 [hep-ph].

[24] ATLAS Collaboration, *Performance of jet substructure techniques for large-R jets in proton-proton collisions at* $\sqrt{s} = 7$ *TeV using the ATLAS detector*, JHEP **09** (2013) 076,
arXiv: 1306.4945 [hep-ex].

[25] ATLAS Collaboration,
Identification of hadronically-decaying, boosted vector bosons in ATLAS at $\sqrt{s} = 13$ *TeV*,
ATL-PHYS-PUB-2015-033 (2015), URL: https://cds.cern.ch/record/2041461.

[26] ATLAS Collaboration, *Identification of boosted, hadronically decaying W bosons and comparisons with ATLAS data taken at* $\sqrt{s} = 8$ *TeV* (2015), arXiv: 1510.05821 [hep-ex].

[27] ATLAS Collaboration,
Flavor Tagging with Track Jets in Boosted Topologies with the ATLAS Detector,
ATL-PHYS-PUB-2014-013 (2014), URL: https://cds.cern.ch/record/1750681.

[28] ATLAS Collaboration, *Measurement of the muon reconstruction performance of the ATLAS detector using 2011 and 2012 LHC proton–proton collision data*,
Eur. Phys. J. **C74**.11 (2014) 3130, arXiv: 1407.3935 [hep-ex].

[29] M. Cacciari, G. P. Salam and G. Soyez, *The Catchment Area of Jets*, JHEP **0804** (2008) 005,
arXiv: 0802.1188 [hep-ph].

[30] M. Cacciari and G. P. Salam, *Pileup subtraction using jet areas*, Phys. Lett. **B659** (2008) 119,
arXiv: 0707.1378 [hep-ph].

[31] ATLAS Collaboration, *Public plots: Impact parameter resolution data 2011* (2012), URL:
http://atlas.web.cern.ch/Atlas/GROUPS/PHYSICS/IDTRACKING/PublicPlots/ATL-COM-PHYS-2012-471/.

[32] A. J. Larkoski, I. Mount and D. Neill, *Power Counting to Better Jet Observables*,
JHEP **12** (2014) 009, arXiv: 1409.6298 [hep-ph].

[33] J. Thaler and K. Van Tilburg, *Identifying Boosted Objects with N-subjettiness*,
JHEP **03** (2011) 015, arXiv: 1011.2268 [hep-ph].

[34] A. J. Larkoski, D. Neill and J. Thaler, *Jet Shapes with the Broadening Axis*, JHEP **04** (2014) 017, arXiv: 1401.2158 [hep-ph].